Journal of Biomedical Optics

SPIEDigitalLibrary.org/jbo

Dynamic model of thermal reaction of biological tissues to laser-induced fluorescence and photodynamic therapy

Alexey Yu. Seteikin
Ilya V. Krasnikov
Eleni Drakaki
Mersini Makropoulou

SPIE

Dynamic model of thermal reaction of biological tissues to laser-induced fluorescence and photodynamic therapy

Alexey Yu. Seteikin,[a,b] Ilya V. Krasnikov,[b] Eleni Drakaki,[c] and Mersini Makropoulou[c]
[a]Kwangwoon University, Electrophysics Department, Wolgye-Dong 447-1, Nowon-GU, 139701 Seoul, Republic of Korea
[b]Amur State University, Physics Department, Ignat'evskoe shosse 21, 675027 Blagoveshchensk, Russia
[c]National Technical University of Athens, School of Applied Mathematical and Physical Sciences, Physics Department, Zografou Campus, 15780 Athens, Greece

Abstract. The aim of this work was to evaluate the temperature fields and the dynamics of heat conduction into the skin tissue under several laser irradiation conditions with both a pulsed ultraviolet (UV) laser ($\lambda = 337$ nm) and a continuous-wave (cw) visible laser beam ($\lambda = 632.8$ nm) using Monte Carlo modeling. Finite-element methodology was used for heat transfer simulation. The analysis of the results showed that heat is not localized on the surface, but is collected inside the tissue in lower skin layers. The simulation was made with the pulsed UV laser beam (used as excitation source in laser-induced fluorescence) and the cw visible laser (used in photodynamic therapy treatments), in order to study the possible thermal effects. [DOI: 10.1117/1.JBO.18.7.075002]

Keywords: simulations; biophotonics; lasers in medicine; thermal effects.

Paper 12794RR received Dec. 13, 2012; revised manuscript received Jun. 8, 2013; accepted for publication Jun. 11, 2013; published online Jul. 9, 2013.

1 Introduction

Novel and noninvasive spectroscopic diagnostic methods have been introduced in biomedical research and applications, e.g., laser-induced fluorescence (LIF) and diffuse reflectance, which could generate an image contrast between different states of skin tissue for basal cell carcinoma or other skin malignancies.[1–3] The biophotonics methods are noninvasive, meaning that they do not require tissue sample excision (biopsy), which is necessary in histopathology characterization and biochemical analysis of skin tissue samples, worldwide used as the diagnosis "gold standard." The *in vivo* spectral fluorescence measurements of human skin can also serve as a valuable supplement for diagnosing various skin diseases, such as venous ulcers, skin necrosis, and interstitial edema.[4–9] Additionally, LIF spectroscopy can be used to produce a "map" for the localization and quantification of the photosensitizers in photodynamic therapy (PDT) of skin cancer, as well as to predict the value of the light intensity distribution in the place of its action.[6–9] The skin contains several fluorescent chromophores (fluorophores) such as nicotinamide adenine dinucleotide reduced form, elastin, collagen, and keratin, which contribute to the fluorescence spectrum, as well as purely absorbing chromophores such as melanin and hemoglobin.[3,8,9]

There are many factors apart from the light fluence affecting the efficacy of PDT. Among all these factors, local tissue temperature during PDT is one of the most important.[10] The absorbed optical energy during PDT generates heat, which also can act synergistically with PDT.[11]

Apart from LIF and PDT, many laser applications in medicine produce heat-inducing changes in the tissue, leading to alterations in the optical properties of the tissue.[10,12] Such alterations will result in redistribution of light within the tissue, and in particular, the penetration of the light within the tissue may be reduced.[10,12]

Optical properties have been shown to be temperature dependent over a physiological temperature range, and are expected to vary from the ultraviolet (UV) to the near-infrared spectrum and across different types of tissues, such as skin and fat. Researchers have shown that fluorescence intensity decreases with increasing temperature, due to the increase of scattering and absorption coefficients.[13–15]

Fluorescence also varies with temperature in a variety of substances. Bowen and Sahu showed that the fluorescence yield of some fluorescent solutions varied inversely with temperature.[16] The dependence of fluorescence intensity on temperature has been attributed to intersystem crossing, or temperature-dependent internal conversion, a process that competes with fluorescence to return excited molecules back to their ground state.[17]

Certain proteins in tissues, such as collagen, which are important biological fluorophores, undergo denaturation and conformational changes at temperatures above body temperature (37°C), and these conformational changes can cause a change in fluorescence. Lipids also undergo documented phase changes that affect optical properties and fluorescence at temperatures above body temperature.[18,19] Therefore, it is very important to know the temperature distribution in skin layers and to predict and measure all these alterations for better monitoring of photodetection and PDT procedures. Experimental techniques for the laser-induced temperature changes recording usually involve an infrared camera. The infrared camera, however, only monitors the temperature of the really superficial layer of the skin, while in deeper-lying tissue the temperature could actually be different. Optical methods of monitoring tissue temperature during simulated skin PDT treatments were also proposed,[10] by using crystals with temperature-dependent

Address all correspondence to: Alexey Yu. Seteikin, Kwangwoon University, Electrophysics Department, Wolgye-Dong 447-1, Nowon-GU, 139701 Seoul, Republic of Korea. Tel: +8229408656; Fax: +74162394525; E-mail: seteikin@mail.ru

0091-3286/2013/$25.00 © 2013 SPIE

fluorescence properties. In addition, temperature distribution in the tissue does not depend solely on heat conduction, but also to a large extent on the light distribution in the tissue.[20] In connection with difficulties associated with experimental data acquisition, it is expedient to use physical and mathematical modeling for laser-induced thermal effects.[21–25]

Monte Carlo–simulated laser energy deposition inside tissue may also be used to compute light dosage for PDT of various diseases. In the previous published works, the utility of Monte Carlo modeling was evaluated for measuring the light intensity distribution in skin samples excited with a pulsed UV laser beam[26] and the diffusion approximation modeling for light intensity distribution in the skin samples with a continuous wave (cw) visible laser beam ($\lambda = 632.8$ nm).[27] Several approaches have been proposed for the optical propagation modeling, e.g., a seven flux model,[28] the Kubelka–Munk theory,[29] the Beer–Lambert law, or a Monte Carlo method.[22] However, there are not many studies on thermal modeling.

This research aims to investigate the tissue thermal response to laser irradiation before an LIF or PDT application in dermatology to minimize the possible adverse effects and complications associated with the laser intervention. A multilayer model based on the physical structure of human skin is employed to predict the temperature distribution of living tissues when they are treated with lasers. We performed Monte Carlo simulation in the UV and visible light distribution and in the distribution of the heat induced by the irradiation.

2 Materials and Methods

2.1 *Simulated Laser Excitation Sources*

The mathematical modeling was carried out on human skin tissue samples under two laser irradiation conditions. (a) The skin samples were irradiated with a pulsed nitrogen laser, emitting at $\lambda = 337$ nm, with an energy output of 0.5, 1, 5, and 10 mJ per pulse, 1 Hz pulse repetition rate, and 4 and 7 ns pulse width. The excitation wavelength around 340 nm is considered to be optimal for inducing autofluorescence from endogenous skin chromophores, resulting in fluorescence emission covering all the visible range. (b) The skin samples were irradiated with a cw He–Ne laser, emitting at $\lambda = 632.8$ nm. The laser's power output values considered in this study were 0.5, 1, 5, and 10 mW, while the irradiation time was 120 s. The mathematical model used a Gaussian, contact to skin tissue, beam, with diameter of 2 mm, chosen for both wavelengths, while the chosen energy fluence and the power fluence values indicated in this article are within the range that is used during PDT.

2.2 *Monte Carlo Simulation*

This method simulates the "random walk" of photons in the human skin tissue volume considering light absorption and scattering. In MC simulation, the skin is treated as a multilayer (five-layer) medium triangulated by 1955 elements. Each layer is characterized by the anisotropy factor g, the absorption coefficient μ_a, scattering coefficient μ_s, refractive index n, effective absorption coefficient μ_d, and thickness d (see Table 1). For each layer, the optical properties were assumed to be invariable, i.e., the model was symmetric in relation to a shift in a plane parallel to the layer interface.

When a photon is scattered, the photon trajectory is deflected by an angle θ in the interval $(0, \pi)$. The probability density function that Henyey and Greenstein originally proposed for galactic light scattering approximates Mie scattering by particles comparable in size to the wavelengths of light, and is given by[31,32]

$$p(\theta) = \frac{1}{4\pi} \cdot \frac{1 - g^2}{(1 + g^2 - 2g\cos\theta)^{3/2}}. \quad (1)$$

The anisotropy factor g is distributed in the interval $(-1, 1)$. A value of 0 indicates isotropic scattering, a value near 1 indicates a very forward-directed scattering, and a value of -1 indicates a fully backward-directed scattering.

For the purpose of this study, we took the optical properties of human skin tissue at 337 and 632.8 nm published by Tuchin.[30] The modeled tissue had the same dimensions as the measured, in the previous work,[27] samples. Photons reaching the outer surface of the sample were modeled as at an air/tissue boundary. For the convenience of simulation, the area of interest of the skin is assumed to be a cylinder with plane parallel layers of 5-mm radius, and the center of the top layer of the cylinder is exposed to a laser beam with a diameter of 2 mm. In Table 1, the optical properties of the five-layered skin at laser excitation of 337 and 632.8 nm are summarized. The software allows simulating a flat and a Gaussian profile of incident laser beam. In this work, a Gaussian profile of laser beam was simulated.

The statement of the method and the basic equations for the Monte Carlo modeling of temperature distribution in the five-layer human skin were described in Refs. 30–35. The distribution of the density of absorbed light energy in tissue,

Table 1 Optical properties of skin at 337 nm laser excitation.[30]

		μ_a(cm^{-1})		μ_s(cm^{-1})		g			
No.	Wavelength (nm)	337	632.8	337	632.8	337	632.8	n	d (cm)
1	Epidermis	32	4.3	165	107	0.72	0.79	1.5	0.01
2	(Papillary) dermis	23	2.7	227	187	0.72	0.82	1.4	0.02
3	Dermis with plexus superficialis	40	3.3	246	192	0.72	0.82	1.4	0.02
4	(Reticular) dermis	23	2.7	227	187	0.72	0.82	1.4	0.09
5	Dermis plexus profundus	46	3.4	253	194	0.72	0.82	1.4	0.06

Q [$Q(\mathrm{J/cm^3})$], is one of the results of MC simulation, which is used in the heat transfer simulation.

The above algorithm allows simulating the continuous action of laser radiation on the biomaterial. However, the obtained value of the light energy distribution in the depth of tissue [$\mathrm{J/cm^3}$] is easily converted to a distribution of the absorbed power [$\mathrm{W/cm^3}$], knowing the power of source. Simple calculations allow obtaining the absorbed power for the nanosecond pulse regime of irradiation.

2.3 *Heat Transfer Simulation*

When laser radiation interacts with matter, a part of the absorbed light energy is finally transferred to heat. The energy is distributed over the volume of the medium rather than localized on the boundary, as is the case of conventional thermal heating. The optical energy is nonuniformly released into the interaction volume, because the light intensity decreases when light penetrates deeper into the medium. The thermal properties of skin vary between different layers; even within the same layer, there exists large nonhomogeneity and anisotropy due to the presence of blood vessels. Both the physiological processes and thermal properties of skin are influenced by a variety of factors such as temperature, damage, pressure, and age.[36]

The finite-element method was used to simulate the temperature fields and the dynamics of heat conduction into the skin tissue under the previously mentioned laser irradiation conditions. Generally, the modeling of nonstationary thermal processes in a cell requires solving of the nonstationary differential heat equation in cylindrical coordinate system:

$$\rho c \frac{\partial T}{\partial t} = k\nabla^2 T + Q, \tag{2}$$

where k is the coefficient of heat conductivity [$\mathrm{J/(m \cdot K)}$], Q is the heat source ($\mathrm{J/m^3}$), ρ is the density ($\mathrm{kg/m^3}$), and c is the heat capacity [$\mathrm{J/(kg \cdot K)}$], with the boundary conditions describing the interaction of a tissue with environment (see Table 2). The distribution of the density of absorbed light energy in tissue or the heat source, Q, is one of the results of MC simulation.

Equation (2) requires initial and boundary conditions. On the bottom side of the skin model (bottom side of dermis plexus profundus layer), the following boundary condition takes place:

$$T|_\Gamma = 37°\mathrm{C}, \tag{3}$$

where Γ corresponds to the boundary of skin. As shown previously,[30] for a healthy person the temperature stabilizes at 450-μm depth. This is caused by thermal regulation produced by blood capillaries and is the second heat drainage (internal) localized on the bottom side of the modeled skin, the first being on the skin surface.

The interaction of the external skin surface (epidermis layer) with environment (convection, radiation) in linear form can be described by boundary conditions of a third type:

$$\left[k\frac{\partial T}{\partial z} - A(T - T_{\mathrm{ext}})\right]\Big|_\Gamma = 0, \tag{4}$$

where $A[\mathrm{W/m^2 \cdot K}]$ is the parameter of convection and T_{ext} is the temperature of the external environment.

When convection is taken into account, the initial temperature of the tissue has a gradient: from 34°C on the surface to 37°C on the skin rear border. Calculations of temperature distribution within multilayered biological tissues are based on our earlier papers.[33–35]

Heat transfer is a dynamic task, thus the Crank–Nicholson scheme was used to solve time-dependent heat-transfer equation in time domain.[37]

3 Results and Discussion

Self-developed (on C#) software based on modified Lihong algorithm for Monte Carlo method[31,32] was used to calculate the 2-D density of absorbed light energy distribution in the skin. Another self-developed algorithm in Matlab was also used for the calculations of heat transfer task.[33–35] Each MC calculation took 1 to 2 min on a Samsung R700 notebook (Intel Core2Duo, 1.83 GHz); the heat transfer task took 5 to 20 min at the same configuration due to large time scale of the task.

The software has been validated by comparing the results of simulation of diffuse reflectance (Rd) for a semi-infinite scattering medium with known analytical results tabulated by Giovanelli results of adding-doubling method, Monte Carlo method based on well-known Wang algorithm (MCML), object-oriented MC (O3MC), and peer-to-peer Monte Carlo (P2PMC) code.[38] The results of comparison are presented in Table 3. The parameters of the medium are: $\mu_s = 9\ \mathrm{mm^{-1}}$, $\mu_a = 1\ \mathrm{mm^{-1}}$, $g = 0$, and $n = 1.5$.

Figure 1(a) and 1(b) shows the results of modeling for time variations of the temperature at the indicated tissue depths of the beam center upon exposure to laser pulses (for an exposure time of 4 and 7 ns and a cooling period of 1 s). The initial data were: the nitrogen laser provided pulses of 4 or 7 ns pulse width at the excitation wavelength $\lambda = 337$ nm, the energy output was 5 mJ

Table 2 Thermal properties of skin.[30]

No.	Layer	k(W/m · K)	c(J/kg · K)	ρ(kg/m^3)
1	Epidermis	0.266	3700	1600
2	(Papillary) dermis	0.498	3200	1200
3	Dermis with plexus superficialis	0.530	3600	1100
4	(Reticular) dermis	0.498	3200	1200
5	Dermis plexus profundus	0.530	3600	1100

Table 3 The results of total diffuse reflectance (Rd) given by analytical results, adding-doubling method, Monte Carlo method based on well-known Wang algorithm (MCML), O3MC, P2PMCa, and our software for 5×10^4 photon packets.[38]

Reference	Rd	SD
Giovanelli	0.26000	—
Adding-doubling	0.26079	0.00170
MCML	0.25907	0.00079
O3MC	0.25957	0.00043
Our software	0.26003	0.00038
P2PMC	0.25977	0.00023

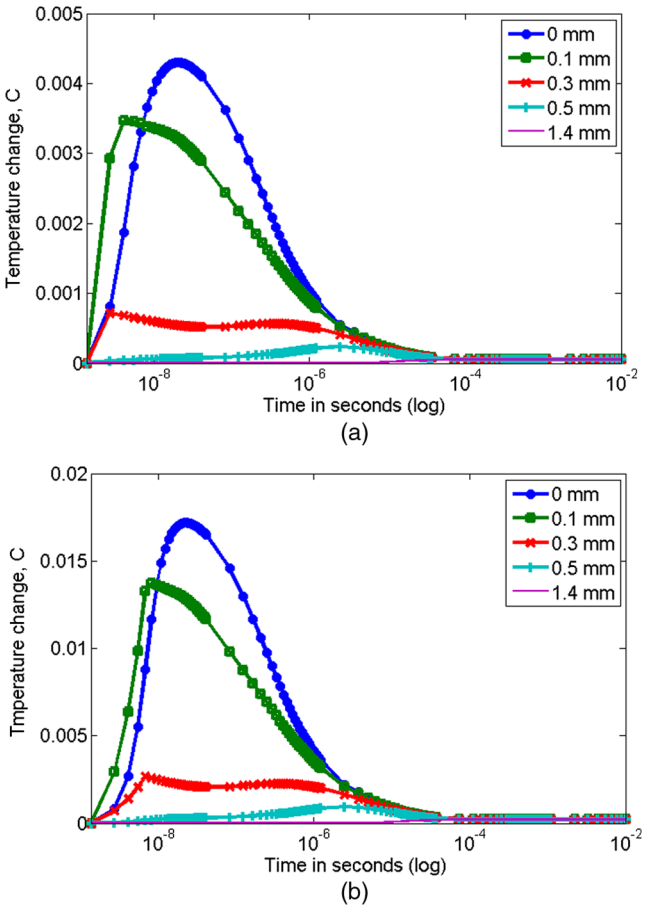

Fig. 1 Skin temperature at the indicated tissue depths of the beam center upon exposure to 4 ns laser pulse (a) or 7 ns laser pulse (b), without convection at the skin surface ($\lambda = 337$ nm, $d = 2$ mm). The indicated depths are related to the depth of each layer from the skin surface.

per pulse and 1 Hz pulse repetition rate, while the laser beam diameter was estimated at 2 mm and thus the energy density is 0.15 J/cm^2.

Figure 2 demonstrates the temperature change in the skin versus depth from the laser beam center ($r = 0$). The biggest part of light energy was absorbed in upper layers (peaks at 0.005 cm), due to their high absorption coefficient at the 337-nm wavelength. The dramatic temperature decrease at 0.01 cm is in accordance with density of absorption energy in tissue and due to the high heat transfer coefficient of dermis. As indicated by dashed lines in Figs. 2 and 3, the shape and the shoulders of the temperature curves follow the layered structure of the model-tissue, thus showing the absorbing properties of the first three tissue layers.

For a possible explanation, the skin optical properties (Table 1) were correlated with the thermal ones (Table 2), where a similar behavior was shown. Light at 337 nm has an optical penetration depth down to approximately 150 μm, at the vicinity of papillary dermis, as was shown with Monte Carlo simulation in the previous work.[26] Fluorophores excited by 337-nm light (within the skin volume) emit a characteristic fluorescence for each fluorophore. As the fluorescence photons travel through the tissue back to the surface, part of the light with longer wavelengths will be reabsorbed by various chromophores within the tissue. It can be concluded that the incident radiation is almost completely absorbed by the uppermost layers, while

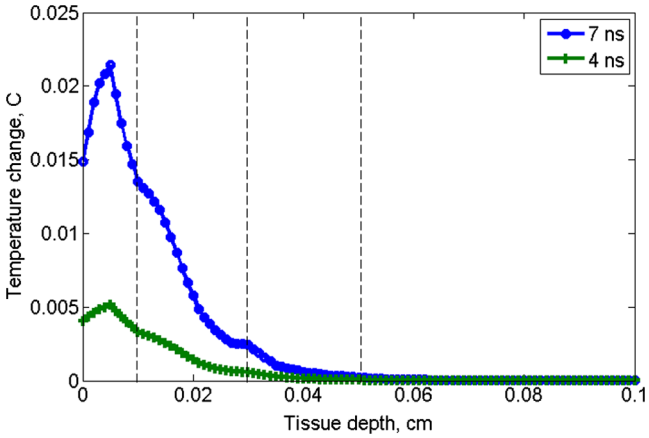

Fig. 2 Skin temperature versus tissue depth from the laser beam center ($r = 0$) upon exposure to 4 and 7 ns laser pulses, after $t = 10$ ns without convection at the skin surface ($\lambda = 337$ nm, $d = 2$ mm).

other spectral components are absorbed in a relatively thick (100 μm) epidermal layer reaching dermis. As was expected, the shorter laser pulse width results in lower temperature rise.

Figure 3(a) and 3(b) represents the temperature change due to absorbed light energy in skin tissue, after 10 ns, versus tissue depth and radial distance from the laser beam center. The initial data were: the nitrogen laser provided pulses of 7 ns pulse width at the excitation wavelength $\lambda = 337$ nm, the energy output was 1 mJ [Fig. 3(a)] and 10 mJ [Fig. 3(b)] per pulse, and 1 Hz pulse repetition rate, while the laser beam diameter was estimated at 2 mm and thus the energy density is 0.03 and 0.32 J/cm^2.

The simulation of the temperature fields and dynamics of heat conduction into the skin tissue was performed for a laser-based diagnostic application. The LIF, with a pulsed UV laser used as excitation source, demonstrated no significant increase of temperature in skin, as shown in Figs. 1–3. The depth to which the radiation of 337 nm penetrated the skin, limited the depth from which temperature variations could be obtained. In the UV spectral region, the penetration depth of light in tissue is approximately 225 μm at 337 nm.[39] The optical penetration depth limits the depth of heat induction.

In Fig. 4, the temperature distribution on skin versus tissue depth and radial distance from the laser beam center, after irradiation with an 10 mW He Ne laser light ($\lambda = 632.8$ nm), after 120 s of irradiation with convection on skin surface is shown. The temperature maximum is allocated inside the tissue on depth 0.2 to 0.6 mm. The temperature on surface does not exceed 41°C.

By using MCML,[27,29] the light distribution of a Gaussian (at 632.8 nm) beam, which falls normally onto skin surface (data not shown) was simulated. Upon processing the data, 14% absorption of 633 nm laser irradiation into the skin sample at the first layer, epidermis, is noticed, while at the papillary dermis and at the reticular dermis 15% and 23%, respectively, of the irradiation is absorbed.

In Fig. 4, it can be seen that the temperature distribution follows the behavior of the fluence distribution. Temperature decreases rapidly as the beam propagates in the skin tissue. Scattering and absorption of the medium induce heat localized diffusion to a certain depth, while the higher transmittance and the lower scattering of the skin tissue at 632.8 nm than at 337 nm allowed the formation of local heat maximum at a considerable depth (>100 μm).

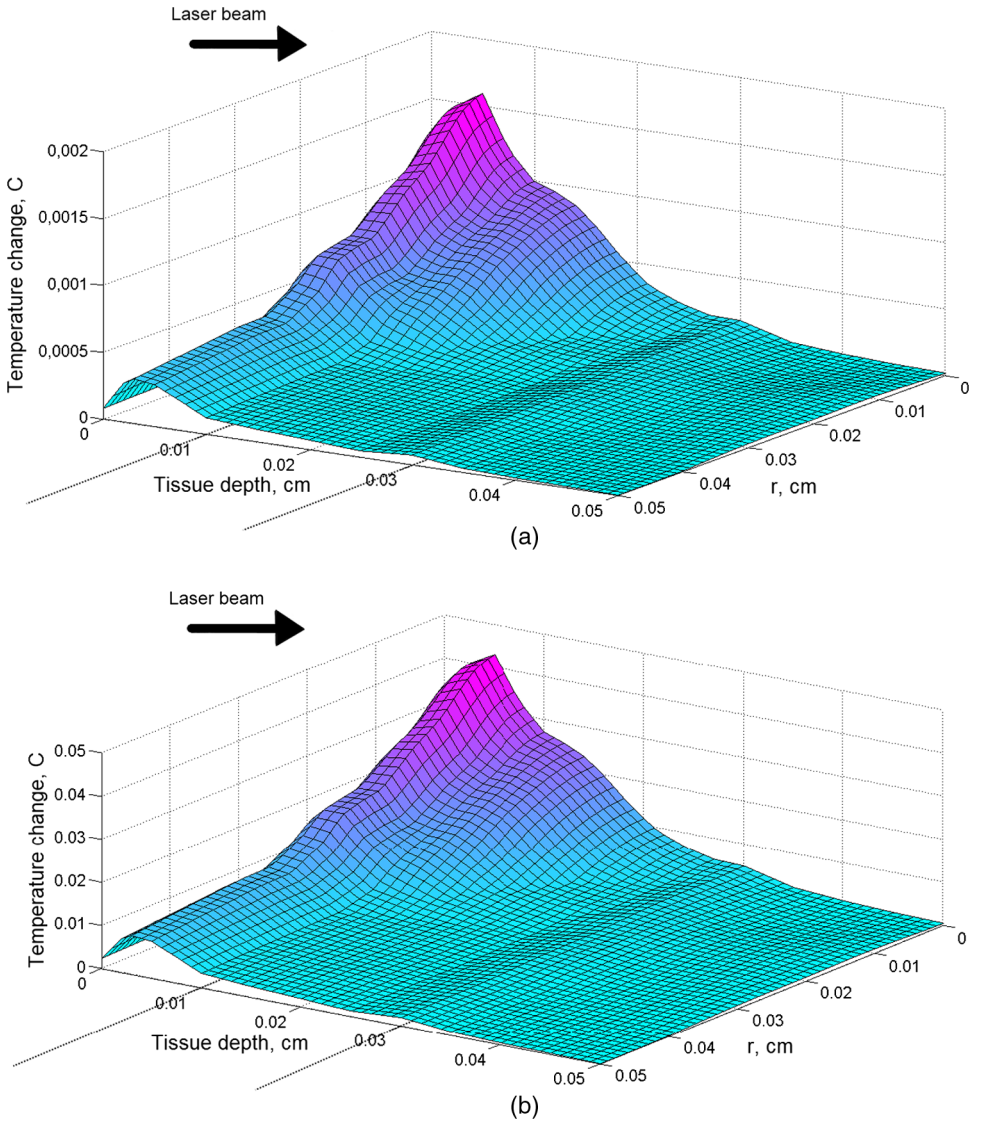

Fig. 3 Temperature rise in skin tissue, after 10 ns, versus tissue depth and radial distance from the laser beam center, without convection at the skin surface ($\lambda = 337$ nm, $d = 2$ mm, $tp = 4$ ns). Laser energy: 1 mJ (a) and 10 mJ (b).

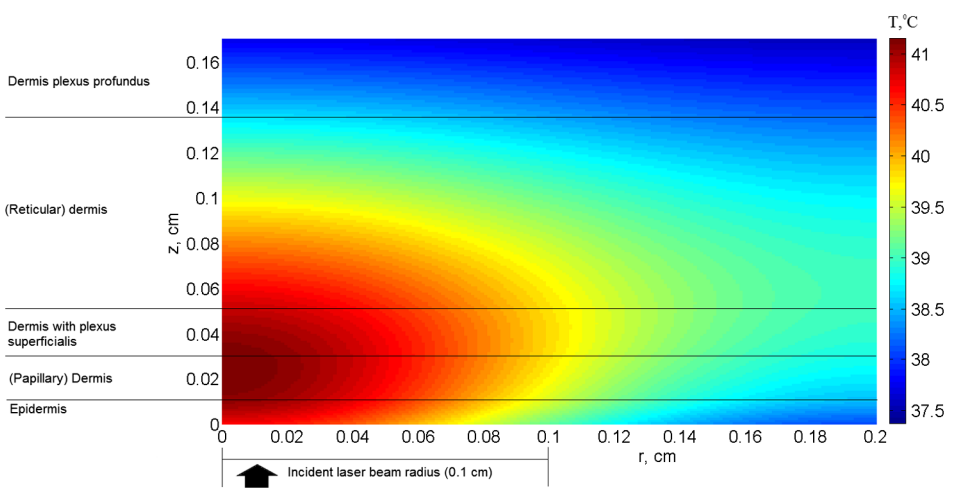

Fig. 4 Temperature distribution versus tissue depth and radial distance from the laser beam center, after 120 s, with convection at the skin surface ($\lambda = 632.8$ nm, $d = 2$ mm). $P = 10$ mW.

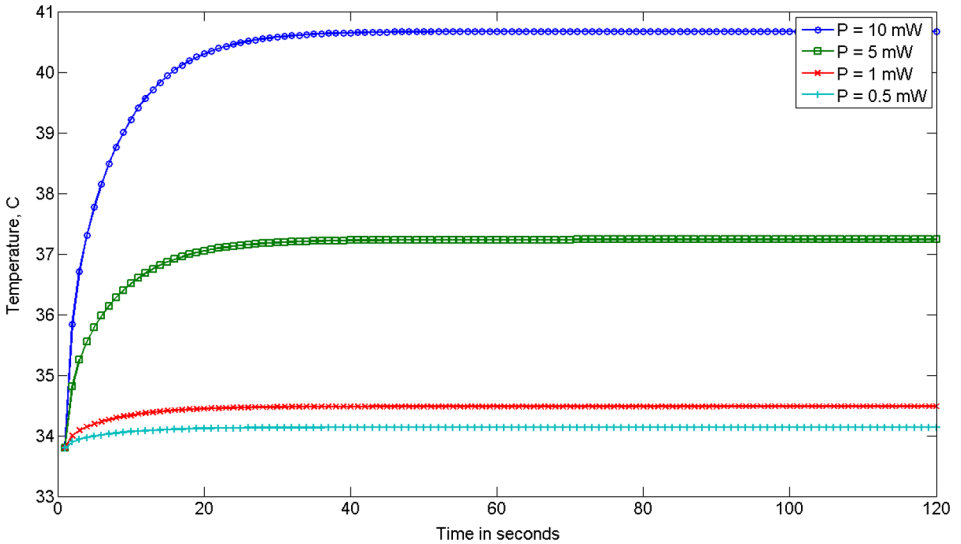

Fig. 5 Temperature dynamic on skin surface with different laser power values, $\lambda = 632.8$ nm, $d = 2$ mm, $P = 0.5$; 1; 5; 10 mW.

As follows from the shown curves (Fig. 5), starting the 20th second after irradiation, the increased temperature stabilizes. In addition to the laser power at the maximum temperature on the surface of the skin also affects the process of convection due to boundary condition mentioned in Eq. (4) of the heat transfer simulation in Sec. 2.3 (results not presented on figure).

It can be observed for both the UV and visible laser irradiation that the temperature maximum is not localized on the surface but inside the skin tissue (Figs. 2–4). The absorption of laser light by tissue strongly depends on wavelength. The absorption coefficient is very high on 337-nm wavelength, so the penetration depth of light is very small. Thus, the absorption of light on 632.8-nm wavelength is 10 times lower and laser light penetration depth is about 10 to 20 mm inside skin (see Table 1).

Under real conditions, besides considered internal heat drainage, the skin has at least one mechanism of temperature regulation: convection on the skin surface [boundary condition (4)]. It represents skin cooling by heat transfer to the ambient medium (air). In this paper, the parameter of convection, A, is set to 100 (W/m^2 K).[30–32,39] Such a mechanism corresponds to skin–air thermal interaction. The drainage can be intensified or inhibited by the application of different substances onto skin surface. For instance, sweat/water evaporation can increase the amount of energy transferred from skin to environment. Thus, considerable amounts of energy accumulated within the modeled skin will be transferred by two drainages, and initial temperature of skin will have a gradient ranging from ~34°C (on the skin surface) to 37°C (deep in skin).

By varying the parameter of convection, A, temperature increases inside the tissue without simultaneous significant thermal damage can be reached (results not presented). For example, by the 20th second of continuous exposure to laser radiation, the temperature on the surface exceeds 40°C (Fig. 5). Normally, the power density of a PDT treatment light when employing surface illumination is low enough not to cause any significantly increased tissue temperature.[36] An another important temperature regulation system is the blood perfusion. In this paper, we simplify blood perfusion in tissue by boundary condition (3), equal to 37°C.

Researchers exhibited the experiments with fluence values much higher than 100 mW/cm^2, in order to notice the important temperature changes for the tissue surface irradiance and hyperthermia effects.[40–43] Many groups, in order to be able to discriminate between photochemical effects and hyperthermic effects and to perform controlled studies, had utilized fluence rates that are below the threshold of hyperthermia.

No significant effect may be found in applications of fluorescence under UV excitation for *in vivo* diagnosis of disease, as normal body temperatures do not vary widely.

At 514 nm, it has been demonstrated by Svaasand that for power densities <150 mW/cm^2, no hyperthermic effects were contributing.[44]

de Bruijn showed in her research[45] that the fluorescence increase in time after illumination with 633 nm using 100 J/cm^2, at 100 mW/cm^2 was temperature dependent. During illumination, the fluorescence bleached to 35%, 43%, 49%, and 49% of the initial fluorescence intensity in tumor, arterioles, venues, and normal tissue, respectively.[45] On the other hand, Warloe et al.[46] detected the skin surface temperature during PDT using aminolevulinic acid (ALA-PDT) with laser light at 630 nm. With a fluence rate of 100 to 150 mW/cm^2, they noticed, like us, a temperature rise to 39°C to 40°C occurred during the first minutes, followed by stabilization at 37°C to 38°C. This is in agreement with the suggestion of Svaasand et al.,[47] who said that a typical incident optical dose for PDT with red light at 630 to 635 nm is around 100 J/cm^2. This dose can easily be obtained without exceeding the threshold for hyperthermia, e.g., with an irradiance of 100 mW/cm^2 for 1000 s (17 min).

Other researchers, using light of 100 mW/cm^2 from a noncoherent light source (590 to 700 nm) including approximately 25% infrared light (1250 to 1550 nm) to human skin and skin tumors, noticed a temperature increase from 39.5°C to 42.5°C in tumor and from 42°C to 43.5°C in normal tissue.[48]

A major concern in the simulation was to design such a model that would sufficiently take into account the features and nature of skin tissue. It would enable the reliable simulation of irradiative and heat processes, which could be a good alternative for time-consuming and very expensive physical phantoms. However, in recent years some authors have made progress in investigations using tissue phantoms.[49,50]

The mathematical models had to make assumptions and simplifications in order to make the problem tractable, while capturing the essential features of the processes. All biological systems are complex, multicomponent, and spatially structured, and their elements have individuality in the optical properties, which had to be taken into consideration for the tissue mathematical model for light distribution. In addition adjustments had to be taken in the bioheat model concerning equilibration site and heat exchange between blood and tissue, blood perfusion, vascular architecture, blood temperature, variation in thermal properties, and blood flow rate. However, temperature rise during laser irradiation is not the only issue for concern: free radicals are also a side effect, positive or negative depending on purpose of laser treatment (e.g., positive for cancer therapy and negative for cosmetic applications).[51,52]

4 Conclusions

In this paper, we consider the distribution of light absorbed density and temperature dynamics in UV and visible laser irradiated skin before an LIF or PDT application. We simulated continuous and pulsed laser influence.

When laser light interacts with tissue, the produced heat is not localized on the surface, but it is collected inside the tissue. When the pulse duration and the cooling period are chosen properly, the biotissue temperature does not exceed the critical temperature even for a long enough exposure time (several minutes). For the pulse duration 4 ns, the maximum temperature rise does not exceed 0.005°C and 0.02°C for 7-ns pulses. By varying the boundary conditions on the surface [Eqs. (3) and (4)] and the type of the laser radiation (continuous or pulsed), we can reach higher than normal temperature inside the tissue, without simultaneous formation of thermally damaged tissue.

Since no permanent tissue damage seems to be done in an *in vivo* study due to the physiological temperatures used, it can be inferred that the loss in fluorescence is completely reversible over this temperature range.

Acknowledgments

The present research has been conducted under a Research Grant from Kwangwoon University in 2012.

References

1. M. Panjehpour et al., "Laser-induced fluorescence spectroscopy for in vivo diagnosis of non-melanoma skin cancers," *Lasers Surg. Med.* **31**(5), 367–373 (2002).
2. E. Borisova et al., "Diagnostics of pigmented skin tumors based on laser-induced autofluorescence and diffuse reflectance spectroscopy," *Quantum Electron.* **38**(6), 597–605 (2008).
3. E. Drakaki et al., "Laser induced fluorescence and reflectance spectroscopy for the discrimination of basal cell carcinoma from the surrounding normal skin tissue," *Skin Pharmacol. Physiol.* **22**(3), 158–165 (2009).
4. R. Eichhorn et al., "Early diagnosis of melanotic melanoma based on laser-induced melanin fluorescence," *J. Biomed. Opt.* **14**(3), 034033 (2009).
5. A. Saarnak et al. "Influence of tumour depth, blood absorption and autofluorescence on measurements of exogenous fluorophores in tissue," *Lasers Med. Sci.* **13**(1), 22–31 (1998).
6. D. Y. Churmakov, I. V. Meglinski, and D. A. Greenhalgh "Amending of fluorescence sensor signal localization in human skin by matching of the refractive index," *J. Biomed. Opt.* **9**(2), 339–346 (2004).
7. I.V. Meglinski and D.Y. Churmakov "Spatial localization of biosensor fluorescence signals in human skin under the effect of equalization of the refractive index of the surrounding medium," *Opt. Spectrosc.* **96**(6), 946–951 (2004).
8. D. Y. Churmakov et al., "Analysis of skin tissues spatial fluorescence distribution by the Monte Carlo simulation," *J. Phys. D: Appl. Phys.* **36**(14), 1722–1728 (2003).
9. R. Cubeddu et al., "Fluorescence lifetime imaging: an application to the detection of skin tumors," *IEEE J. Sel. Top. Quantum Electron.* **5**(4), 923–929 (1999).
10. J. W. Pickering et al., "Changes in the optical properties (at 632.8 nm) of slowly heated myocardium," *Appl. Opt.* **32**(4), 367–371 (1993).
11. W. M. Star, B. C. Wilson, and M. S. Patterson "Light delivery and optical dosimetry in photodynamic therapy of solid tumors," in *Photodynamic Therapy: Basic Principles and Clinical Applications*, T. J. Dougherty, B. C. Wilson, and B. W. Henderson, Eds., pp. 335–367, Marcel Dekker, NY (1992).
12. N. Yavari "Optical spectroscopy for tissue diagnostics and treatment control," Doctoral Thesis, Department of Physics and Technology, University of Bergen, Norway (2006).
13. D. Barton "Variation of fluorescence with temperature in human tissue," Master of Science Thesis, Biomedical Engineering, Vanderbilt University, Nashville, Tennessee (2010).
14. M. G. Müller et al., "Intrinsic fluorescence spectroscopy in turbid media: disentangling effects of scattering and absorption," *Appl. Opt.* **40**(25), 4633–4646 (2001).
15. J. Wu, M. S. Feld, and R. P. Rava "Analytical model for extracting intrinsic fluorescence in turbid media," *Appl. Opt.* **32**(19), 3585–3595 (1993).
16. E. J. Bowen and J. Sahu "The effect of temperature on fluorescence of solutions," *J. Phys. Chem.* **63**(1), 4–7 (1959).
17. W.-C. Lin, M. Motamedi, and A. J. Welch "Dynamics of tissue optics during laser heating of turbid media," *Appl. Opt.* **35**(19), 3413–3420 (1996).
18. J. Laufer et al., "Effect of temperature on the optical properties of ex vivo human dermis and subdermis," *Phys. Med. Biol.* **43**(9), 2479–2489 (1998).
19. J. M. Menter "Temperature dependence of collagen fluorescence," *Photochem. Photobiol. Sci.* **5**(4), 403–410 (2006).
20. P. van der Zee, "Measurement and modeling of the optical properties of human tissue in the near infra-red," Dissertation, University College London, UK (1992).
21. S. W. Zhang, J. Fuqian, and Y. Fuqian "Three-dimensional model on thermal response of skin subject to laser heating," *Comput. Methods Biomech. Biomed. Eng.* **8**(2), 115–125 (2005).
22. S. Jacques and L. Wang "Monte Carlo modeling of light transport in tissue," in *Optical-Thermal Response of Laser-Irradiated Tissue*, A. J. Welch and M. J. C. Van Gemert, Eds., pp. 73–100, Plenum Press, NY (1995).
23. V. K. Pustovalov et al., "Thermal processes during the interaction of optical radiation pulses with heterogeneous biotissues," *Int. J. Heat Mass Transfer* **33**(5), 771–784 (1990).
24. V. K. Pustovalov and B. Jean "Thermooptical comparison of different approaches and lasers for laser treatment of intraocular tumors," *Laser Phys. Lett.* **1**(7), 368–372 (2004).
25. V. Venugopalan, N. S. Nishioka, and B. B. Mikić, "Thermodynamic response of soft biological tissues to pulsed infrared-laser irradiation," *Biophys. J.* **70**(6), 2981–2993 (1996).
26. E. Drakaki, M. Makropoulou, and A. Serafetinides "In vitro fluorescence measurements and Monte Carlo simulation of laser irradiation propagation in porcine skin tissue," *Lasers Med. Sci.* **23**(3), 267–276 (2008).
27. M. Makropoulou et al., "A diffusion approximation model of light transport in multilayered skin tissue," *Proc. SPIE* **6628**, 662818 (2007).
28. W. Vargas "Two-flux radiative transfer model under nonisotropic propagating diffuse radiation," *Appl. Opt.* **38**(7), 1077–1085 (1999).
29. L. F. Gate "Comparsion of the photon diffusion model and Kubelka–Munk equation with the exact solution of the radiative transport equation," *Appl. Opt.* **13**(2), 236–238 (1974).
30. V. V. Tuchin, Ed., *Handbook of Photonics for Biomedical Science*, CRC Press, Taylor & Francis Group, London (2010).
31. L.-H. Wang, S. L. Jacques, and L.-Q. Zheng "MCML-Monte Carlo modeling of photon transport in multi-layered tissues," *Comput. Methods Prog. Biomed.* **47**(2), 131–146 (1995).
32. L.-H. Wang, S. L. Jacques, and L.-Q. Zheng "CONV-convolution for responses to a finite diameter photon beam incident on multi-layered tissues," *Comput. Methods Prog. Biomed.* **54**(3), 141–150 (1997).

33. A. Y. Seteikin and I. V. Krasnikov "Research on thermal influence of laser radiation on skin with non-trivial geometry," *Proc. SPIE* **6826**, 68260N (2008).
34. A. Y. Seteikin and I. V. Krasnikov "The analysis of the thermal effects arising at interaction of laser radiation with the multilayered biomaterial by using Monte Carlo method," *Proc. SPIE* **6595**, 659520 (2007).
35. A. Y. Seteikin and I. V. Krasnikov "An analysis of thermal effects resulting from laser radiation interaction with a multilayered biotissue," *Russ. Phys. J.* **49**(10), 1139–1144 (2006).
36. J. Svensson et al., "Tissue temperature monitoring during interstitial photodynamic therapy," *Proc. SPIE* **5698**, 126–136 (2005).
37. C. Zienkiewicz and K. Morgan, *Finite Elements and Approximation*, John Wiley & Sons, New York (1983).
38. A. Doronin and I. Meglinski "Peer-to-peer Monte Carlo simulation of photon migration in topical applications of biomedical optics," *J. Biomed. Opt.* **17**(9), 090504 (2012).
39. N. Ramanujam "Fluorescence spectroscopy of neoplastic and non-neoplastic tissues," *Neoplasia* **2**(1–2), 89–117 (2000).
40. M. Niemz, *Laser Tissue Interactions: Fundamentals and Applications*, Springer, Berlin, Heidelberg, New York (1996).
41. A. Szasz, N. Iluri, and O. Szasz, "Local hyperthermia in oncology—to choose or not to choose?," *Hyperthermia*, InTech, Croatia (2013).
42. R. Sorensen, V. Iani, and J. Moan, "Kinetics of photobleaching of protoporphyrin IX in the skin of nude mice exposed to different fluence rates of red light," *Photochem. Photobiol.* **68**, 835–840 (1998).
43. T. M. Sitnik and B. W. Henderson, "The effect of fluence rate on tumor and normal tissue responses to photodynamic therapy," *Photochem. Photobiol.* **67**, 462–466 (1998).
44. L. O. Svaasand "Photodynamic and photohyperthermic response of malignant tumors," *Med. Phys.* **12**(4), 455–461 (1985).
45. H. S. de Bruijn "Light fractionated ALA-PDT," Ph.D. Thesis, Erasmus Universiteit Rotterdam, Holland (2008).
46. T. Warloe et al., "Photochemotherapy of multiple basal cell carcinoma with endogenous porphyrins induced by topical application of 5-aminolevulinic acid," in *Photodynamic Therapy and Biomedical Lasers*, P. Spinelli, M. Dal Fante, and R. Marchesini, Eds., pp. 449–453, Elsevier Science Publishers B.V., Amsterdam (1992).
47. L. O. Svaasand et al., "Light and drug distribution with topically administered photosensitizers," *Lasers Med. Sci.* **11**(4), 261–265 (1996).
48. A. Orenstein et al., "Temperature monitoring during photodynamic therapy of skin tumors with topical 5-aminolevulinic acid application," *Cancer Lett.* **93**(2), 227–232 (1995).
49. A. V. Bykov et al., "Skin phantoms with realistic vessel structure for OCT measurements," *Proc. SPIE* **7376**, 73760F (2010).
50. A. V. Bykov et al., "Multilayer tissue phantoms with functioning capillary system for OCT and DOCT imaging," *Proc. SPIE* **8091**, 80911R (2011).
51. A. P. Popov et al., "Effect of size of TiO2 nanoparticles applied on glass slide and porcine skin on generation of free radicals under ultraviolet irradiation," *J. Biomed. Opt.* **14**(2), 021011 (2009).
52. I. V. Krasnikov et al., "Influence of titanium dioxide nanoparticles on skin surface temperature at sunlight irradiation," *Biomed. Opt. Express* **2**(12), 3278–3283 (2011).